ADVANCED OPTICAL MATERIALS
www.advopticalmat.de

# Controlling Plasmonic Chemistry Pathways through Specific Ion Effects

*Andrei Stefancu, Lin Nan, Li Zhu, Vasile Chiș, Ilko Bald, Min Liu, Nicolae Leopold,* Stefan A. Maier, and Emiliano Cortes**

Dedicated to Professor Jochen Feldmann on the occasion of his 60th birthday

**Plasmon-driven dehalogenation of brominated purines has been recently explored as a model system to understand fundamental aspects of plasmon-assisted chemical reactions. Here, it is shown that divalent $Ca^{2+}$ ions strongly bridge the adsorption of bromoadenine (Br-Ade) to Ag surfaces. Such ion-mediated binding increases the molecule's adsorption energy leading to an overlap of the metal energy states and the molecular states, enabling the chemical interface damping (CID) of the plasmon modes of the Ag nanostructures (i.e., direct electron transfer from the metal to Br-Ade). Consequently, the conversion of Br-Ade to adenine almost doubles following the addition of $Ca^{2+}$. These experimental results, supported by theoretical calculations of the local density of states of the Ag/Br-Ade complex, indicate a change of the charge transfer pathway driving the dehalogenation reaction, from Landau damping (in the lack of $Ca^{2+}$ ions) to CID (after the addition of $Ca^{2+}$). The results show that the surface dynamics of chemical species (including water molecules) play an essential role in charge transfer at plasmonic interfaces and cannot be ignored. It is envisioned that these results will help in designing more efficient nanoreactors, harnessing the full potential of plasmon-assisted chemistry.**

## 1. Introduction

Until recently, the plasmonic chemistry community focused mainly on Landau damping as the primary electron/energy transfer from plasmonic nanostructures to adsorbed molecules.[1–4] In the context of surface plasmon resonance, Landau damping represents the scattering of hot electrons (electrons with energy greater than the thermal energy) at the surface of nanostructures[5] (thus, it scales with $1/R$ for spherical nanostructures, where $R$ is the radius[6,7]). Nonetheless, despite the enormous efforts and advances to increase the efficiency of chemical reactions through Landau damping, the efficiency of such reactions remains low. The low efficiency is mainly due to the unavoidable losses in the metals (provided by bulk scattering, electron-electron scattering, and thermalization of hot electrons), which often surpass the energy gain provided by the plasmon resonance modes.[8–10]

Therefore, the plasmonic community started slowly to shift focus from Landau damping to chemical interface damping (CID) as the primary pathway for electron/energy transfer from plasmonic nanostructures to adsorbates.[11–13] Contrary to Landau damping, which is a multistep effect (first, the electrons are excited above the Fermi level, then they are scattered at the surface of the nanostructures, where

A. Stefancu, L. Nan, L. Zhu, S. A. Maier, E. Cortes
Chair in Hybrid Nanosystems
Nanoinstitute Munich
Faculty of Physics
Ludwig-Maximilians-Universität München
80539 Munich, Germany
E-mail: emiliano.cortes@lmu.de

A. Stefancu, V. Chiș, N. Leopold
Faculty of Physics
Babeș-Bolyai University
Cluj-Napoca 400084, Romania
E-mail: nicolae.leopold@ubbcluj.ro

The ORCID identification number(s) for the author(s) of this article can be found under https://doi.org/10.1002/adom.202200397.



**DOI: 10.1002/adom.202200397**

I. Bald
Institute of Chemistry
Physical Chemistry
University of Potsdam
14476 Potsdam, Germany

M. Liu
State Key Laboratory of Powder Metallurgy
School of Physical and Electronics
Central South University
Changsha 410083, China

S. A. Maier
Department of Physics
Imperial College London
London SW7 2AZ, UK

S. A. Maier
School of Physics and Astronomy
Monash University
Clayton Victoria 3800, Australia

they can be transferred to adsorbed molecular orbitals), CID represents the direct electron transfer from the Fermi level to the adsorbate energy state, conditioned by an overlap between the metal states and the adsorbate states (i.e., hybridization).[14,15] It was shown recently that CID can lead at least to the same charge transfer efficiency as Landau damping and even become the dominant charge transfer mechanism in some systems.[14]

Nonetheless, a prerequisite for both Landau- and CID-assisted charge transfer to molecules is for the molecules to be adsorbed closely to the surface of the plasmonic nanostructures or adsorbed directly on it, in the case of CID. In the surface-enhanced Raman scattering (SERS) effect for example (which requires the same condition, since the electromagnetic fields decay with $r^{-10}$ from the metal surface[16]), the low adsorption affinity of many target molecules is a well-known hurdle toward their sensitive detection. Examples of this include glucose (whose direct label-free SERS spectrum was not yet achieved),[17] water molecules[18,19] (with very modest enhancement factors despite the fact that most SERS studies are done in aqueous solvents), or organic acids,[20] among other examples. The surface effects which deal with the dynamics of chemical species at the surface of nanostructures usually receive very little attention compared to Landau damping or CID. However, as in the above examples regarding SERS detection, such surface effects and surface dynamics often dictate the interaction between molecules and nanostructures and cannot simply be ignored or assumed negligible.

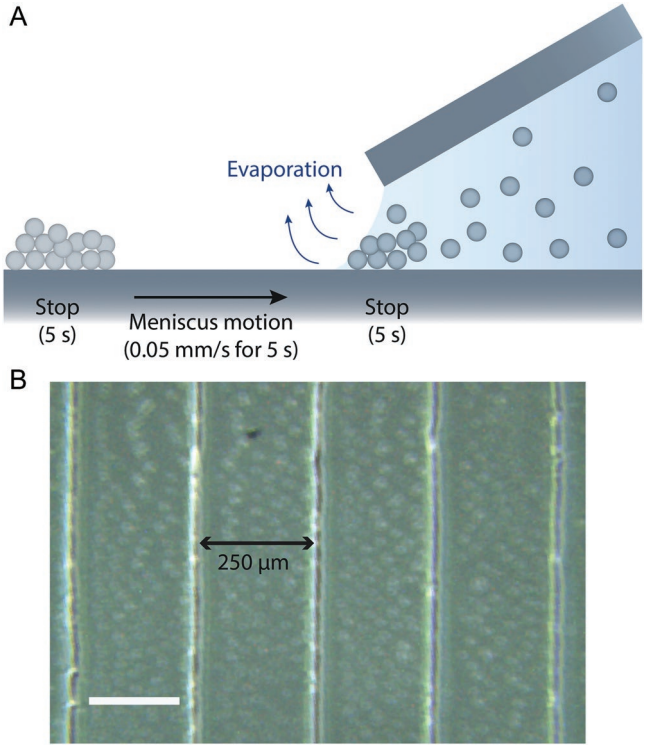


**Figure 1.** Characterization of the AgNW substrates. A) Scheme of the stop-and-go process for synthesizing the AgNW (additional details in the Experimental Section). B) Optical image of a representative AgNW substrate. The scale bar represents 200 µm.

Our recent SERS studies[21–23] provide evidence that specific ion effects control the selective adsorption of molecules onto colloidal silver nanoparticles (AgNPs). As a rule of thumb, the addition of positively ($Ca^{2+}$, $Mg^{2+}$), or negatively ($Cl^-$, $Br^-$) charged ions[18,19,24,25] leads to the selective adsorption of negatively and positively charged molecules, respectively on the surface of AgNPs. Most often, the Derjaguin-Landau-Verwey-Overbeek (DVLO) theory is used to model the interactions of ions with colloidal nanoparticles (NPs) and surfaces in general. However, the predictions of the DVLO model are often refuted by experiments which show that certain ions interact specifically with colloidal nanoparticles and surfaces, leading thus to specific ion effects.[26–28]

In this study, we aim to explore such specific ion effects in the plasmon-assisted dehalogenation reaction of 8-bromoadenine (Br-Ade) to adenine (Ade) on Ag surfaces. As far as we know, the way in which specific ion effects impact plasmon-assisted reaction rates has never been studied before. The dehalogenation of Br-Ade to Ade has been studied extensively by the Bald group[29–34] and, importantly, a thermal-driven reaction has been excluded through power-dependent measurements as well as in studies using nanosecond laser pulses, suggesting that the main electron transfer pathway from AgNPs to Br-Ade is a plasmon-assisted one. This is also confirmed by a recent study using in situ electrochemical SERS.[35]

Here we show that divalent $Ca^{2+}$ and $Mg^{2+}$ ions increase the dehalogenation rate of Br-Ade by specifically bridging its adsorption on silver nanowires (AgNW) and thus increasing the adsorption affinity of Br-Ade to the Ag surface. Contrary, monovalent $Na^+$ does not affect the reaction rate. These experimental results show conclusively how specific ion effects and the dynamics of chemical moieties at the NPs surface impact plasmon-assisted chemical reactions at the nanoscale. Moreover, based on these results, we can indirectly suggest which plasmon-assisted charge transfer mechanism dominates, since Landau damping and CID should be affected differently by the surface chemistry and surface effects.

## 2. Results and Discussions

We start first by characterizing the nanosubstrate used throughout this study. Silver nanowires (AgNW) were synthesized from concentrated citrate capped AgNPs colloidal solution (obtained through the Lee-Meisel method[36]) through convective self-assembly[37] (CSA). To obtain the AgNWs separated by a well-defined distance, we used the stop-and-go method[38] (more details in the Experimental Section).

**Figure 1** shows schematically the synthesis process, together with a representative optical image of the obtained substrate. Figure S1 in the Supporting Information, shows that the SERS intensity of Ade adsorbed on the AgNW is uniform across the surface of the AgNW, thus offering a reproducible substrate for testing the Br-Ade dehalogenation.

Next, we monitored the SERS intensity of Br-Ade with and without $Ca^{2+}$ (in the form of $Ca(NO_3)_2$ salt) by using the AgNW substrate. We show in **Figure 2**A,B that the adsorption affinity of Br-Ade for the Ag surface increases significantly in the presence of $Ca^{2+}$, leading consequently to an increase of the

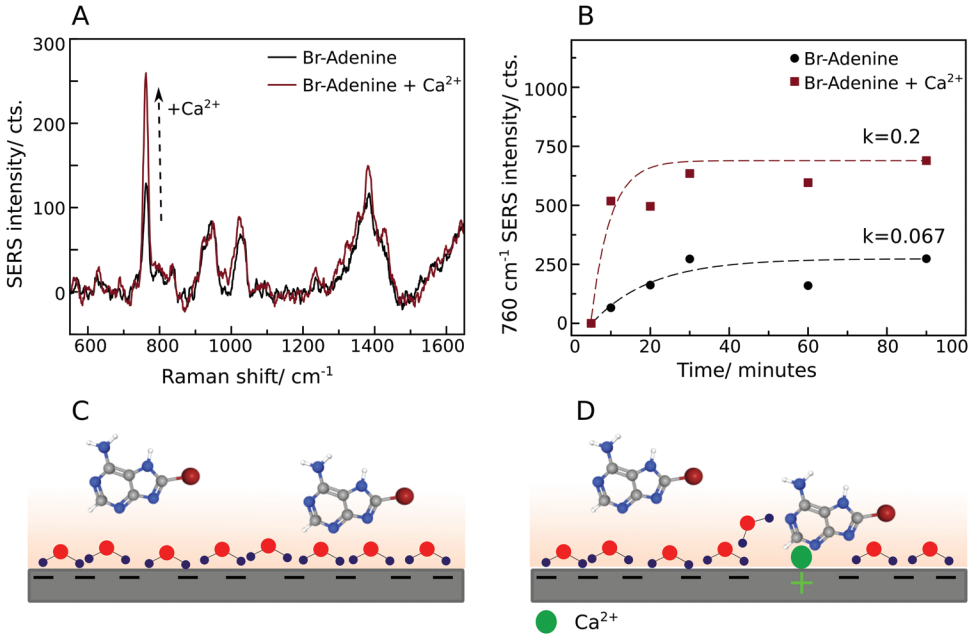


**Figure 2.** A) A representative example of the increase of Br-Ade SERS intensity following the addition of $Ca^{2+}$. The SERS spectra were taken with the 785 nm laser, on the AgNW substrate. B) The increase of the SERS intensity of 760 $cm^{-1}$ SERS peak of Br-Ade on AgNW with and without $Ca^{2+}$, monitored in time, at 785 nm excitation (1 s integration time, 9 mW). Due to the low integration time and high time-spacing between acquisitions (i.e., minutes), no dehalogenation of Br-Ade occurred. The time-dependent SERS intensity was fitted with a Langmuir curve (the dotted lines), yielding the adsorption constants of Br-Ade with $Ca^{2+}$ ($k = 0.2$) and without $Ca^{2+}$ ($k = 0.067$). C) Schematic view of the adsorption of Br-Ade on the Ag surface without $Ca^{2+}$ and D) with the addition of $Ca^{2+}$, which leads to surface charge reversal locally. The shaded orange region represents the hydration layer of the Ag surface, while the negative charge of the Ag surface is given by the citrate surfactant.

SERS intensity of Br-Ade. For monitoring the time-dependent SERS intensity of Br-Ade, the AgNW substrate immersed in a Br-Ade solution with and without $Ca^{2+}$, respectively, was placed under the Raman microscope and SERS spectra were acquired, periodically, from the same spot on the AgNW. Since the acquisition time of each SERS spectrum was 1 s (laser power 9 mW) and the time gap between consecutive acquisitions was on the order of minutes, no dehalogenation reaction of Br-Ade was observed (i.e., the decrease in the intensity of 760 $cm^{-1}$ peak and increase in the 730 $cm^{-1}$ SERS peak). Figure S2 in the Supporting Information, shows the increase of the SERS intensity of Br-Ade after the addition of $Ca^{2+}$ on two other substrates, confirming the increased adsorption affinity of Br-Ade after the addition of $Ca^{2+}$. These results are in line with previous SERS studies on the selective adsorption of positively and negatively charged molecules on AgNPs, due to adsorbed ions.[22,23] Moreover, in Figure S3 in the Supporting Information, we show the calculated adsorption energy of Br-Ade on Ag(111) with and without $Ca^{2+}$. The adsorption energy increases from −0.58 to −1.05 eV upon the addition of $Ca^{2+}$ ions.

At this point, we can start suggesting possible mechanisms for the results observed in Figure 2. Let us consider for a moment the structure of the electrical double layer at the Ag surface, and the mechanism of adsorption of like-charged molecules. A negatively charged Ag surface (due to the citrate surfactant) will adsorb charged ions, specifically and nonspecifically. Specifically adsorbed ions can possess a chemical or specific affinity for the Ag surface, whereas the nonspecifically adsorbed ions are attracted to the surface by purely Coulombic forces.[39] The plane defined by the specifically adsorbed ions defines the inner Helmholtz plane, while the hydrated ions adsorbed on the surface define the outer Helmholtz plane. Together they define the first layer of the electrical double layer.[39,40] The second layer is called the diffuse layer and is located further away from the surface.[40] The presence of cationic species, such as $Ca^{2+}$, has been shown to decrease the magnitude of the negatively charged surface's zeta potential (which quantifies the variations in the electric double layer's charge) by increasing the positive charge density located in the first electrical double layer.[40]

Let us consider now the adsorption of Br-Ade to the negatively charged Ag surface, shown schematically in Figure 2C,D. Due to the presence of the bromide atom, the charge distribution of Br-Ade changes compared to Ade (as shown by the molecular electrostatic potential maps in Figure S5, Supporting Information) leading to a change in the dipole moment of Br-Ade compared to Ade. For adsorption to occur, Br-Ade must overcome Coulombic repulsion via hydrophobic interactions or be facilitated by the screening of counterions. If the attraction of Br-Ade to the surface overcomes repulsive forces, then the adsorption proceeds in time. Thus, within this framework, we can interpret our SERS results (and dark field scattering (DFS) results shown in Figure 5) as follows. $Ca^{2+}$ ions increase the positive charge density in the first electric double layer at the AgNW surface, and thus decrease the Coulombic repulsion between the negatively charged Ag surface and Br-Ade, bridging the specific adsorption of Br-Ade. In fact, divalent ions such as $Ca^{2+}$ or $Mg^{2+}$ have been shown to reverse the local surface's

charge (an effect called charge reversal), whereas monovalent ions such as $Na^+$ or $K^+$, cannot counteract the surface's charge, although they increase the positive charge density in the first electrical double layer.[41] In our case, the citrate capping layer of the AgNPs did not influence the adsorption of Br-Ade on AgNPs since there are no strong SERS bands of citrate in the spectra. This suggests that Br-Ade has a stronger affinity for the Ag surface than citrate.

At a more fundamental level, these surface ion specific effects are related to the Hofmeister series, and the local water structure. The Hofmeister series is an empirical sequence describing the efficiency of different salts in precipitating proteins and suspensions in general (such as colloids) and since its report it left physical-chemists eluded as to what dictates this series. The Hofmeister series was then extended to describe interactions of ions with metal and organic surfaces; however, the mechanism remains partially known, at best.[42–44] Until now, the best guess is that ions leave the bulk structure of water intact, however, they modify the local water shell around surfaces or proteins.[42–44] In our case, Collin's law of matching water affinities applies.[45] It states that the hydration shell of two cosmotropic ions may overlap, leading to ion pairing.[45] However, a chaotropic ion may not penetrate the hydration shell of a cosmotropic ion. Consistent with this law, we can assume that strongly hydrated cosmotropic ions, such as $Ca^{2+}$ or $Mg^{2+}$, can penetrate the surface hydration layer of Ag, while weakly hydrated chaotropic ions, such as $Na^+$ or $K^+$, are excluded from the surface layer. Moreover, theoretical and experimental results have suggested that the cosmotropic ions are to some degree dishydrated (or even completely dishydrated), allowing close contact between the bare ion and the surface, analogous to close contact ion pairing between two cosmotropic ions in solution. Therefore, $Ca^{2+}$ ions can bridge the adsorption of Br-Ade very close to the Ag surface.

Next, we bring experimental evidence that $Ca^{2+}$ ions, besides leading to an increase of the SERS intensity of Br-Ade, also increase the conversion of Br-Ade to Ade by a factor of ≈ 2. We acquired time-series SERS measurements with the 785 and 633 nm lasers, for ≈30 s (0.5 s integration time with 0.5 dwell time in-between acquisitions) and tracked the reaction dynamics of Br-Ade to Ade. The intensity of the SERS marker peaks at 760 $cm^{-1}$ (for Br-Ade) and 730 $cm^{-1}$ (for Ade) were used to quantify the conversion rate. The peak at 760 and 730 $cm^{-1}$ were assigned by us to the ring breathing mode of Br-Ade and Ade, respectively, through density functional theory (DFT) calculations (see Tables S1–S3 and Figure S7, Supporting Information, for an in-depth analysis of the Raman modes of Ade and Br-Ade).

**Figure 3** shows the dynamics of Br-Ade to Ade reaction during irradiation with 785 and 633 nm, through the difference

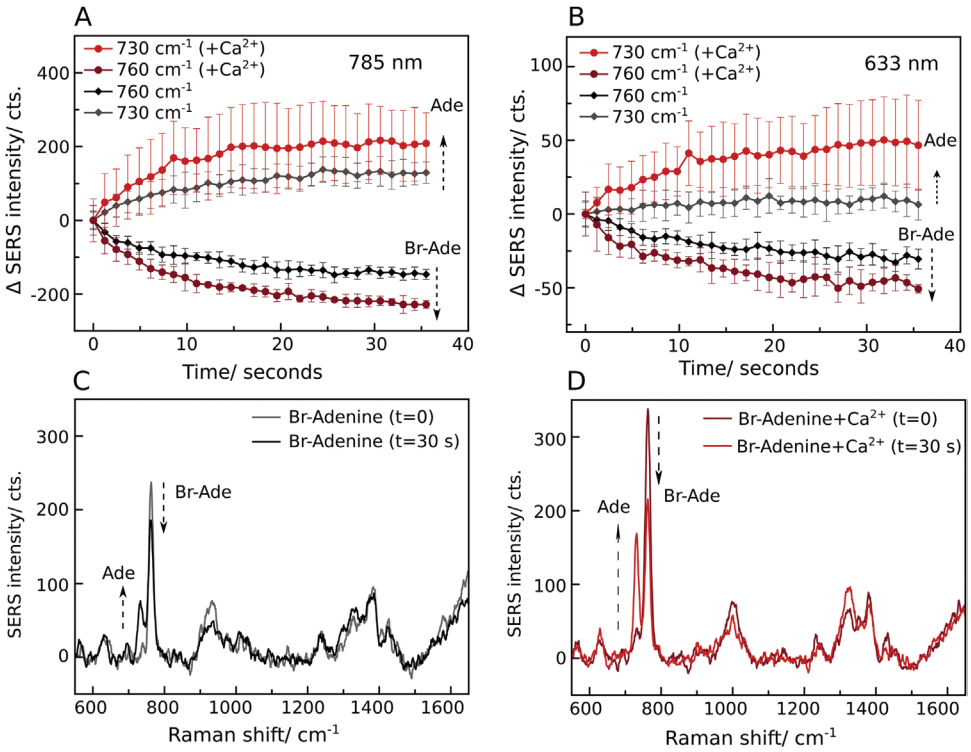


**Figure 3.** The dehalogenation of Br-Ade to Ade monitored through the time evolution of the SERS intensity of 760 and 730 $cm^{-1}$ peaks, respectively. The Δ SERS (i.e., $Intensity_{t>0} - Intensity_{t=0}$) for the 730 and 760 $cm^{-1}$ peaks without $Ca^{2+}$ (gray and black lines, respectively) and with $Ca^{2+}$ added (deep red and light red, respectively) for A) 785 nm and B) 633 nm irradiation. In both cases, the 760 $cm^{-1}$ SERS peak intensity decreases while the 730 $cm^{-1}$ SERS peak intensity increases, corresponding to the conversion of Br-Ade to Ade. Moreover, in both cases, the conversion is significantly greater (almost twice) following the addition of $Ca^{2+}$. The bars represent the standard deviation from five measurements on different AgNW. C,D) Representative SERS spectra (785 nm laser) of the first and last spectrum in the time series measurements, showing a significantly higher conversion rate of Br-Ade to Ade following the addition of $Ca^{2+}$ (D). Also, note the higher SERS intensity of the 760 $cm^{-1}$ peak at $t = 0$ in (D) compared to (C).

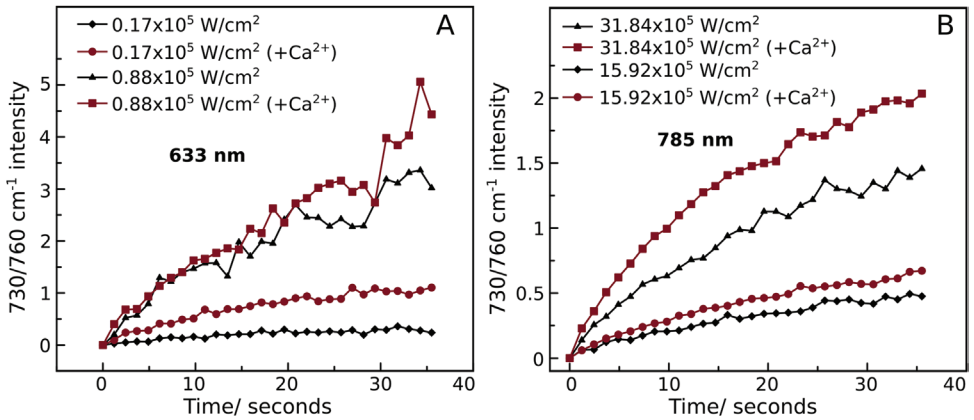


**Figure 4.** The conversion rate of Br-Ade to Ade at A) 633 nm and B) 785 nm excitation, for two laser power densities, quantified through the 730/760 $cm^{-1}$ SERS intensity.

in the SERS intensity of the 730 and 760 $cm^{-1}$ peaks, with and without the addition of $Ca^{2+}$. In addition, Figure S6 in the Supporting Information shows the time-series SERS measurements from two other substrates with 785 nm irradiation, all showing the same outcome: $Ca^{2+}$ increases the conversion of Br-Ade to Ade. Note that, since our analysis was based on the *difference* in the SERS intensity relative to the starting point (noted ΔSERS intensity in Figure 3), the results are independent of the initial SERS intensity of the 760 or 730 $cm^{-1}$ peaks.

Moreover, we determined the conversion rate of Br-Ade to Ade in the presence of different $Ca^{2+}$ concentrations (i.e., $0.5 \times 10^{-3}$ and $0.05 \times 10^{-3}$ M), and found a direct correlation between the $Ca^{2+}$ concentration and the conversion rate (Figure S8, Supporting Information).

Similar results were obtained for bromoguanine, with 785 nm excitation laser (Figure S9, Supporting Information), which was expected given the similar chemical structure of Br-Ade and bromoguanine.

$Mg^{2+}$ addition led to the same results as $Ca^{2+}$, increasing the dehalogenation rate of Br-Ade to Ade (Figure S10, Supporting Information), whereas $Na^{+}$ did not lead to any significant changes (Figure S11, Supporting Information). This further supports the mechanism of divalent cations bridging the adsorption of Br-Ade to the Ag surface.

In order to quantify the dehalogenation rate of Br-Ade, we plotted the 730/760 $cm^{-1}$ SERS intensity, which corresponds to the rate of Br-Ade conversion to Ade for 785 and 633 nm irradiation, at two different laser powers (**Figure 4**). First, it is evident that at 633 nm excitation the conversion rate is higher than at 785 nm, even though the power density is lower. This is due to the higher absorption of the AgNW at 633 nm, compared to 785 nm. Second, the addition of $Ca^{2+}$ increases the Br-Ade to Ade conversion in all cases.

By fitting the experimental curves in Figure 4 with a fractal reaction kinetic model,[46] we determined the reaction rate, *k*, for 633 and 785 nm. For 633 nm ($0.17 \times 10^5$ W $cm^{-2}$) we obtained a reaction rate of 0.023, which increased to 0.07 after the addition of $Ca^{2+}$. Likewise, for 785 nm ($31.84 \times 10^5$ W $cm^{-2}$) we obtained a reaction rate of 0.082, which increased to 0.11 after the addition of $Ca^{2+}$.

However, one must be careful in quantifying the dehalogenation rate through the ratio 730/760 $cm^{-1}$ SERS intensity, since multiple effects can lead to a change in the SERS intensity. Particularly, in our case, for the 785 nm excitation, the decrease of 760 $cm^{-1}$ peak intensity (i.e., Br-Ade dehalogenation) is symmetric with the increase of the 730 $cm^{-1}$ peak intensity (Figure 3A). This suggests that indeed Br-Ade molecules were converted to Ade with a one-to-one ratio. However, for 633 nm excitation (Figure 3B, without $Ca^{2+}$), the decrease of the 760 $cm^{-1}$ peak intensity was always greater than the increase in the 730 $cm^{-1}$ peak intensity. This result hints at a desorption induced by electronic transitions mechanism in addition to the Br-Ade conversion to Ade. Thus, at 633 nm, charge transfer from the Ag surface to Br-Ade will take place, and the kinetic energy of the electrons imparted to Br-Ade molecules is high enough to cause desorption of Br-Ade molecules instead of conversion to Ade, resulting in a skewed time-evolution of the 760 and 730 $cm^{-1}$ SERS intensity. We also note here that by irradiating the AgNW with 633 nm and higher power density ($0.88 \times 10^5$ W $cm^{-2}$), the effects of $Ca^{2+}$ on the dehalogenation rate of Br-Ade are smaller compared to those when using 785 nm excitation (Figure 4A). We suspect that this is a result of two effects: i) thermal effects (which are not affected by surface dynamics are $Ca^{2+}$ ions) could contribute to the dehalogenation of Br-Ade to Ade and ii) Landau damping could become the dominant charge transfer pathway at 633 nm wavelength, whereas at 785 nm in the presence of $Ca^{2+}$ ions CID drives the reaction (see below).

The increased adsorption affinity of Br-Ade to Ag surface following the addition of $Ca^{2+}$ is also observed in the DFS measurements, shown in **Figure 5**. As mentioned in the Introduction, CID represents the direct electron transfer from the surface plasmon resonance to overlapping molecular orbitals. As a result of this new dephasing pathway, the plasmon resonance will decay faster, broadening the plasmon resonance lineshape in the frequency space. Additionally, a redshift and decrease in intensity of the plasmon resonance can be observed' however, this depends also on the local refractive index. Therefore, the broadening of the plasmon resonance is usually considered a more reliable parameter for quantifying the CID.[11]

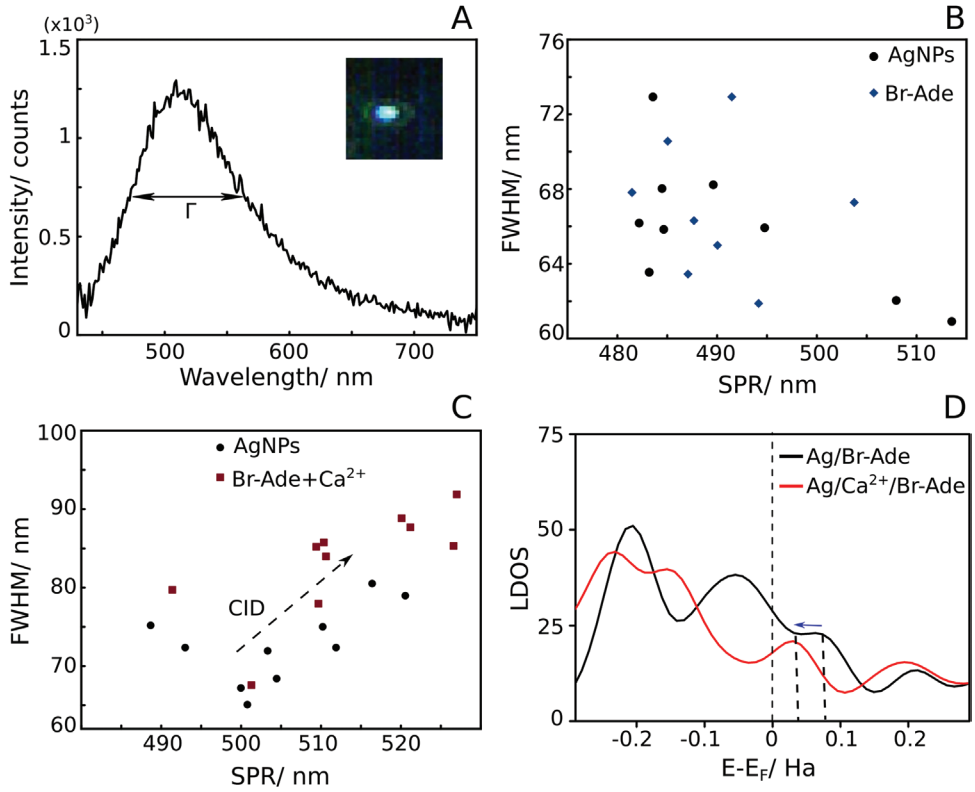


**Figure 5.** Monitoring the adsorption of Br-Ade on AgNPs following the addition of $Ca^{2+}$ by dark field scattering (DFS). A) A typical dark field scattering spectrum of AgNPs (≈ 100 nm diameter) with 40x air objective, after normalization to the lamp spectrum. The scattering spectrum is characterized by a Lorentzian curve, with full-width-at-half-maximum (FWHM), Γ, and resonant wavelength given by the peak of the scattering spectrum. The resonant wavelength and Γ for ten AgNPs before and after adding B) Br-Ade and C) Br-Ade with $Ca^{2+}$. In the case where Br-Ade and $Ca^{2+}$ were added, the AgNPs evidenced a strong CID effect, through the redshift of the resonant wavelength and an increase of the FWHM (C). In contrast, after the addition of Br-Ade alone, no significant differences were observed (B). D) The local density of states (LDOS) of the Ag surface with adsorbed Br-Ade and Br-Ade and $Ca^{2+}$, respectively. A shift of the LDOS of the Ag-Br-Ade complex toward the Fermi level energy can be observed in the presence of $Ca^{2+}$ ions, indicated by the blue arrow.

In Figure 5, we probed the plasmon resonance of ten single AgNPs (≈ 100 nm in diameter) in water and in a solution of Br-Ade and Br-Ade with $Ca^{2+}$, respectively. For the sample containing only Br-Ade, no significant differences were observed in the resonant wavelength or full-width-at-half-maximum (FWHM) of the surface plasmon resonance of AgNPs (Figure 5B). For the sample containing both Br-Ade and $Ca^{2+}$ ions, a significant damping (broadening and redshift) of the surface plasmon resonance was observed (Figure 5C) compared to the single AgNPs in water (see also Figure S12, Supporting Information). This suggests, as in the case of the SERS results presented in Figures 2 and 3, that Br-Ade alone is nonspecifically adsorbed at the surface of the AgNPs and, after the addition of $Ca^{2+}$ (or $Mg^{2+}$), becomes specifically adsorbed, the adsorption being bridged by the $Ca^{2+}$ (or $Mg^{2+}$) ions.

Although the geometry of the AgNW substrates used for the SERS measurements is different from that of the single AgNP used in the DFS experiments, the surface chemistry is the same in both cases. The AgNW were synthesized from citrate capped AgNPs, the same as the AgNPs used in the DFS measurements (additional details in the Experimental Section). Thus, even though the surface plasmon resonance is obviously different on the two nanostructures, the surface dynamics should be very similar.

CID is associated with the direct electron transfer from the Fermi level of AgNPs to acceptor molecular orbitals, when there is an overlap between the metal and molecular energy states (i.e., chemisorption). An increased damping of the surface plasmon resonance, observed in the case of Br-Ade with $Ca^{2+}$, suggests a significant CID caused by Br-Ade, due to the increased adsorption affinity provided by $Ca^{2+}$. Thus, we believe that through $Ca^{2+}$ bridging the adsorption of Br-Ade on Ag surface, Br-Ade shifts from physisorption to chemisorption, facilitating the direct electron transfer from the surface plasmon resonance modes of Ag nanostructures to Br-Ade acceptor orbitals, characteristic of CID. Therefore, the increase in the dehalogenation rate of Br-Ade following the addition of $Ca^{2+}$ is assigned by us to CID (i.e., direct electron transfer transitions), whereas in the lack of $Ca^{2+}$ ions, the dehalogenation reaction is likely driven by Landau damping, as indicated in previous studies[29] (i.e., hot electrons). By the same token, thermal effects can be disregarded since the addition of $Ca^{2+}$ ions would not influence in any way the temperature of the AgNW upon laser irradiation.

This interpretation is also supported by the shift of the local electronic density of states (LDOS) of Ag with Br-Ade and $Ca^{2+}$ toward the Fermi level energy compared to only Ag with Br-Ade calculated theoretically (Figure 5D). Figure 5D shows the LDOS for Ag (111) with adsorbed Br-Ade and Br-Ade-$Ca^{2+}$, respectively,

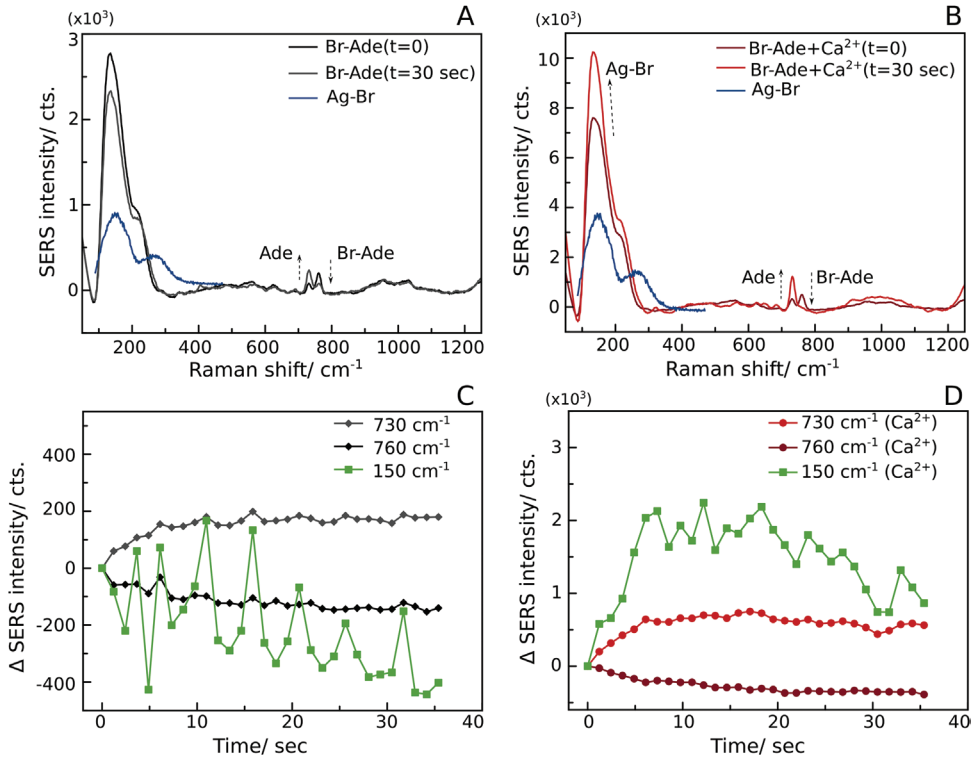


**Figure 6.** The surface dynamics of $Br^-$ ions correlated with the dehalogenation of Br-Ade to Ade. Representative SERS spectra (785 nm laser, 0.5 s acquisition time, and 0.5 s dwell time) of the first and last spectrum in the time series measurements in the 50–1200 $cm^{-1}$ range without A) $Ca^{2+}$ and B) with $Ca^{2+}$, showing an increase of the Ag-Br SERS band at low wavenumbers, correlated to the conversion of Br-Ade to Ade following the addition of $Ca^{2+}$. The blue spectrum represents the SERS band of Ag-Br, with a maximum at ≈ 155 $cm^{-1}$. The Δ SERS intensity (i.e., $Intensity_{t>0} - Intensity_{t=0}$) for the 730, 760, and 150 $cm^{-1}$ peaks C) without $Ca^{2+}$ and D) with $Ca^{2+}$ added. The scatter plot represents the average of three separate measurements.

with respect to the Fermi level energy of Ag. We note first the strong contributions from the electronic d-states of Ag at energies below ≈ −0.11 Ha (corresponding to ≈ −3 eV).[47] Most importantly, above the Fermi level energy the acceptor electronic states of the Ag/Br-Ade complex are observed at ≈ 0.09 Ha (≈ 2.5 eV) which are shifted to ≈ 0.05 Ha (≈ 1.36 eV) above the Fermi level energy (as marked by the blue arrow in Figure 5D). Interestingly, this is very close to the laser energy of the 785 nm laser (≈ 1.5 eV). Therefore, these results could also explain why, at 633 nm excitation, $Ca^{2+}$ ions do not have such a great influence as for 785 nm (see Figure 3).

To further highlight that the Br-Ade dehalogenation to Ade is driven by a metal-molecule electron transfer process, we tracked the conversion rate of Br-Ade to Ade in the presence of a hole scavenger, methanol (Figure S13, Supporting Information). The increase in the conversion rate in the presence of methanol supports our hypothesis that the Br-Ade conversion to Ade is driven by an electron transfer process.

For the dehalogenation of Br-Ade to Ade by metal-molecule charge transfer to take place, a counter reaction is needed to scavenge the holes left behind in the metal. It was previously proposed that the $Br^-$ ions that are cleaved off Br-Ade molecules adsorb to the Ag surface, forming AgBr complexes,[48,49] and act as hole scavengers, facilitating the electron transfer rather than the recombination of the hot electrons with the corresponding holes in the metal states.[50] To validate this counter reaction, and explore the role of $Ca^{2+}$ ions, we tracked the time-dependent intensity of the Ag-Br SERS band at ≈ 150 $cm^{-1}$.[49] If, after cleavage, the $Br^-$ ions are adsorbed on the Ag surface, then we should see an increase in the intensity of the Ag-Br SERS band, correlated with the Br-Ade dehalogenation. Therefore, we acquired time-series SERS measurement of Br-Ade on AgNW at 785 nm, this time in the 50–1200 $cm^{-1}$ wavenumber range.

**Figure 6** shows that on the AgNW with Br-Ade, the Ag-Br SERS band does not change much during the time-series measurement (Figure 6A,C), only decreasing slightly. On the other hand, following the addition of $Ca^{2+}$ ions, the Ag-Br SERS band increases in intensity significantly (Figure 6B,D).

In Figure S14 in the Supporting Information, we show that the Ag-Br SERS peak on AgNW increases after the addition of $Ca^{2+}$, which is consistent with our earlier SERS studies regarding the adsorption of negatively charged chemical moieties on AgNPs.[20–22] This is attributed to the same cation bridging effect discussed above, by which the repulsive Coulombic forces between the $Br^-$ ions and the negatively charged Ag surface are screened by $Ca^{2+}$.

A hurdle for testing this mechanism more conclusively is that in the same wavenumber region, there is another peak, which could possibly stem from plasmonic electronic Raman scattering in the Ag metal.[51] Thus, the peak at low wavenumbers in Figure 6 is probably a convolution of the Ag-Br SERS signal and the electronic Raman scattering from the metal substrate itself. This also explains why the peak at 150 $cm^{-1}$ has such a high intensity. Nonetheless, the plasmonic electronic

scattering peak should be constant in time,[51] thus its observed variation in the presence of $Ca^{2+}$ is most likely due to the increase of the Ag-Br SERS peak.

Interestingly, the variations in the Ag-Br SERS intensity (Figure 6 C,D) could stem from the decomposition of the Ag-Br surface complexes under laser irradiation and the formation of $Br_2$ within a few seconds.

The results of Figures 5 and 6 show that both the stronger adsorption of Br-Ade to the Ag surface and the adsorption of $Br^-$ ions to the Ag surface cooperate to increase the plasmon-assisted dehalogenation rate of Br-Ade to Ade under light irradiation.

Concluding, we show for the first time the impact of specific ion effects, particularly $Ca^{2+}$ and $Mg^{2+}$, in the plasmon-assisted dehalogenation of Br-Ade to Ade. More specifically, we show that divalent $Ca^{2+}$ and $Mg^{2+}$ ions can bridge the adsorption of negatively charged Br-Ade to the negatively charged AgNW surface, and thus facilitate the direct charge transfer from the plasmon resonance modes of Ag nanostructure to the acceptor orbitals of Br-Ade, resulting in the cleavage of the Adenine-Br bond. Based on the DFS measurements, we suggest that CID is the primary electron transfer mechanism driving the dehalogenation of Br-Ade, in the presence of $Ca^{2+}$ ions, due to the stronger adsorption of Br-Ade to the Ag surface, which leads to an overlap of the metal states and molecular energy orbitals, as shown by the calculated density of states (DOS). Contrarily, in the lack of $Ca^{2+}$ ions, Landau damping is probably the main electron transfer mechanism. These results show how complex plasmonic interfaces can be, and that the surface dynamics of molecules and even of water molecules cannot be ignored. By considering connected physical-chemistry aspects of the surface-molecule interaction, such as Hofmeister effects, a more comprehensive understanding of plasmonic chemistry can be achieved, and more efficient strategies can be designed for harnessing the full potential of plasmon-assisted chemical reactions at the nanoscale.

## 3. Experimental Section

*Synthesis of AgNPs and AgNW*: AgNPs capped with citrate anions (cit-AgNPs), synthesized by Lee and Meisel method[36] were used throughout this study. Briefly, the AgNPs were synthesized as follows: in 98 mL ultrapure water, 17 mg $AgNO_3$ were dissolved. The solution was boiled under constant magnetic stirring. At boiling, 2 mL of a trisodium citrate solution (1%) were added dropwise and the solution was left to boil for another hour.

First, 2 mL of the AgNPs colloidal solution was concentrated by centrifugation at 7300 × *g*, for 15 min. The supernatant was discarded by pipetting, and the AgNPs were resuspended in 20 µL ultrapure water. For all films, regular microscopy coverglasses were used as substrate, which was placed in a UV-Ozone cleaner for 15 min prior to the deposition of the AgNW. The UV-Ozone irradiation has a dual role: first, it cleans the coverglass from all organic impurities, and second, it turns the glass surface hydrophilic and decreases the surface tension of the colloidal AgNPs drop, so that it spreads more easily in between the two glass edges. The CSA coater comprised of a motorized translational stage (Thorlabs Inc.) that uses a linear actuator from Thorlabs. A cover glass that acted as a blade was fixed in the near vicinity of the substrate at the desired angle, while the concentrated AgNPs solution was placed on the substrate, underneath, and nearby the edge of the blade. More details about this technique can also be found in ref. [37]. For the deposition of the AgNW, the motorized table was programmed to move in specific sequences. First, the motorized table moves for 250 µm, at a speed of 0.05 mm $s^{-1}$; then, it stops for 5 s, during which the colloidal AgNPs deposit on the coverglass, forming the nanowire. This sequence was then repeated multiple times, to create an optimal number of AgNW. In our case, a separation between AgNW of 250 µm was chosen; however, this can be lowered or increased, depending on the application. The resulting AgNW usually had a width of ≈ 10 µm (Figure S15, Supporting Information).

*DFS Measurements*: Since our DFS setup works in the 400–1000 nm range, larger and more monodisperse spherical AgNPs were synthesized with a diameter of around 100 nm, for which their surface plasmon resonance (SPR) can be measured at around 470 nm. The AgNPs were synthesized according to a previously reported method.[52] Briefly, 30 nm AgNPs were synthesized by mixing 50 mL of water–glycerol mixture (40 vol% glycerol), to which 9 mg of $AgNO_3$ were added and the solution was heated to 95 °C, under vigorous stirring (1000 rpm). When the 95 °C was reached, 1 mL sodium citrate solution (3%) was added, and the solution was heated at 95 °C for 1 h. The obtained 30 nm AgNPs were used as seeds for growing 100 nm AgNPs. In 138 mL $H_2O$, 23 mL of glycerol and 0.58 g polyvinylpyrrolidone (PVP) were added. Then, 2.6 mL of the AgNPs seeds (30 nm) were added, followed shortly (20–30 s) by the addition of 1.15 mL of diamine silver complex (20 mg $AgNO_3$ in 1 mL $H_2O$ and 220 µL ammonium hydroxide 30%) and 92 mL ascorbic acid (36.8 mg). The mixture was mixed at room temperature for 1 h.

The AgNPs were centrifuged at 7300 × *g*, for 15 min, resuspended in ultrapure water and diluted (15 µL of colloidal solution in 1 mL ultrapure water). Then, ≈300 µL of the diluted colloidal solution was pipetted into a microfluidic cell (µ-Slide I Lauer, uncoated microfluidic cell with a channel height of 0.8 mm, purchased from Ibidi, Germany). The microfluidic cell was heated at 50–60 °C until the colloidal solution dried inside the microfluidic channel (≈4–5 h), and the AgNPs were deposited on the bottom of the channel. For the DFS measurements, a home-built microfluidic pump was used to add, sequentially, ultrapure water and Br-Ade or Br-Ade with $Ca(NO_3)_2$, respectively, through the microfluidic cell.[48] After each solution was pumped through the microfluidic cell, the dark field spectra of the same AgNPs were measured. The DFS measurements were performed on a Cytoviva hyperspectral imaging system, using a 40X Olympus microscope objective. After the measurements, the spectra were normalized to the lamp spectrum. The resulting DFS spectra were then fitted in Python, using the curve_fit function (Scipy package) with a Lorentzian curve, and the position of the maximum and FWHM were extracted for each spectrum.

*SERS Measurements*: All SERS measurements were performed on an InVia Raman spectrometer (Renishaw), coupled to a Leica upright microscope. For the SERS measurements on the AgNW, the solid substrate was immersed in 2 mL Br-Ade solution (1 mL of Br-Ade solution of concentration $1 \times 10^{-3}$ M and 1 mL ultrapure water), or Br-Ade + $Ca(NO_3)_2$ (1 mL of Br-Ade solution of concentration $1 \times 10^{-3}$ M, 900 µL ultrapure water and 100 µL $Ca(NO_3)_2$ of $10 \times 10^{-3}$ M concentration) and left for 2 h at room temperature so the Br-Ade can adsorb to the Ag surface. Then, the substrate was removed from the Br-Ade solution, rinsed with ultrapure water, left to dry at room temperature, and placed under the microscope. An exception was the experiments shown in Figure 2, in which the SERS measurements were performed with the substrate still immersed in the Br-Ade solution. The time-series SERS measurements were acquired using a 100x long working distance microscope objective (Olympus, N.A. 0.8). The time-series measurements consisted of 30 acquisitions, with an integration time of 0.5 and 0.5 s between the acquisitions. The 785 nm laser line was provided by a solid-state diode laser, while the 633 nm laser wavelength by a He-Ne laser. The laser power was measured after the microscope objective. The resulting spectra were then automatically processed in Matlab with a home-built script. First, the spectra were smoothed and the background was subtracted. Afterward, the intensity at 760 and 730 $cm^{-1}$ was extracted from each spectrum.

*DOS Calculation*: To explore the specific effect of $Ca^{2+}$ on the dehalogenation of Br-Ade to Ade on Ag(111) surface, a 8 × 4 Ag(111)

periodic surface slab including four atomic layers was built and a 20 Å vacuum slab was added to avoid the influence of the periodic boundary conditions. Each model contains 128 atoms. The DFT calculations were performed by Vienna Ab Initio Simulation Package (VASP) with the projector augment wave method. The exchange and correlation potentials are present in the generalized gradient approximation with the Perdewe–Burkee–Ernzerhof. A $1 \times 2 \times 1$ gamma grid of *K*-points was used for the Brillouin zone integration. The cutoff energy, the convergence criteria for energy and force were set as 450 eV, $10^{-4}$ eV per atom and 0.02 eV $Å^{-1}$, respectively.

## Supporting Information

Supporting Information is available from the Wiley Online Library or from the author.

## Acknowledgements

The authors acknowledge funding and support from the Deutsche Forschungsgemeinschaft (DFG, German Research Foundation) under Germany's Excellence Strategy – EXC 2089/1 – 390776260, the Bavarian program Solar Technologies Go Hybrid (SolTech), the Center for NanoScience (CeNS) and the European Commission through the ERC Starting Grant CATALIGHT (802989). The authors also acknowledge funding by the Romanian Ministry of Research and Innovation, CCCDI-UEFISCDI, project numbers PN-III-P4-ID-PCCF-2016-0112, PN-III-P2-2.1-PED-2019-3268, and PN-III-P4-ID-PCE-2020-1292. The authors thank the Natural Science Foundation of China (Grant Nos. 21872174, 22002189, and U1932148), International Science and Technology Cooperation Program (Grant No. 2017YFE0127800), Hunan Province Key Field R&D Program (2020WK2002), Hunan Provincial Natural Science Foundation of China (2020JJ2041 and 2020JJ5691). S.A.M. additionally acknowledges the Lee-Lucas Chair in Physics.

Open access funding enabled and organized by Projekt DEAL.

## Conflict of Interest

The authors declare no conflict of interest.

## Data Availability Statement

The data that support the findings of this study are available from the corresponding author upon reasonable request.

## Keywords

chemical interface damping, Hofmeister effect, hydration layer, plasmonic chemistry, specific ion effects, surface-enhanced Raman scattering

Received: February 18, 2022
Revised: March 21, 2022
Published online: May 11, 2022

[1] R. Sundararaman, P. Narang, A. S. Jermyn, W. A. Goddard Iii, H. A. Atwater, *Nat. Commun.* **2014**, *5*, 5788.
[2] A. M. Brown, R. Sundararaman, P. Narang, W. A. Goddard, H. A. Atwater, *ACS Nano* **2016**, *10*, 957.
[3] A. J. Leenheer, P. Narang, N. S. Lewis, H. A. Atwater, *J. Appl. Phys.* **2014**, *115*, 134301.
[4] S. Lee, H. Hwang, W. Lee, D. Schebarchov, Y. Wy, J. Grand, B. Auguié, D. H. Wi, E. Cortés, S. W. Han, *ACS Energy Lett.* **2020**, *5*, 3881.
[5] G. V. Hartland, L. V. Besteiro, P. Johns, A. O. Govorov, *ACS Energy Lett.* **2017**, *2*, 1641.
[6] U. Kreibig, M. Vollmer, *Optical Properties of Metal Clusters* (Eds: U. Kreibig, M. Vollmer), Springer, Berlin **1995**, pp. 13–201.
[7] B. Foerster, A. Joplin, K. Kaefer, S. Celiksoy, S. Link, C. Sönnichsen, *ACS Nano* **2017**, *11*, 2886.
[8] J. B. Khurgin, *Nat. Nanotechnol.* **2015**, *10*, 2.
[9] J. Gargiulo, R. Berté, Y. Li, S. A. Maier, E. Cortés, *Acc. Chem. Res.* **2019**, *52*, 2525.
[10] E. Cortés, L. V. Besteiro, A. Alabastri, A. Baldi, G. Tagliabue, A. Demetriadou, P. Narang, *ACS Nano* **2020**, *14*, 16202.
[11] B. Foerster, V. A. Spata, E. A. Carter, C. Sönnichsen, S. Link, *Sci. Adv.* **2019**, *5*, eaav0704.
[12] S. A. Lee, S. Link, *Acc. Chem. Res.* **2021**, *54*, 1950.
[13] E. Oksenberg, I. Shlesinger, A. Xomalis, A. Baldi, J. J. Baumberg, A. F. Koenderink, E. C. Garnett, *Nat. Nanotechnol.* **2021**, *16*, 1378.
[14] J. B. Khurgin, A. Petrov, M. Eich, A. V. Uskov, *ACS Photonics* **2021**, *8*, 2041.
[15] B. N. J. Persson, *Surf. Sci.* **1993**, *281*, 153.
[16] B. J. Kennedy, S. Spaeth, M. Dickey, K. T. Carron, *J. Phys. Chem. B* **1999**, *103*, 3640.
[17] Z. Schultz, *Spectroscopy* **2020**, *35*, 15.
[18] A. Otto, *J. Raman Spectrosc.* **2002**, *33*, 593.
[19] A. Otto, *J. Raman Spectrosc.* **2005**, *36*, 497.
[20] S. D. Iancu, A. Stefancu, V. Moisoiu, L. F. Leopold, N. Leopold, *Beilstein J. Nanotechnol.* **2019**, *10*, 2338.
[21] N. Leopold, A. Stefancu, K. Herman, I. S. Tódor, S. D. Iancu, V. Moisoiu, L. F. Leopold, *Beilstein J. Nanotechnol.* **2018**, *9*, 2236.
[22] A. Stefancu, S. D. Iancu, V. Moisoiu, N. Leopold, *Rom. Rep. Phys.* **2018**, *70*, 509.
[23] A. Stefancu, S. D. Iancu, N. Leopold, *J. Phys. Chem. C* **2021**, *125*, 12802.
[24] A. Otto, A. Bruckbauer, Y. X. Chen, *J. Mol. Struct.* **2003**, *661–662*, 501.
[25] V. Petráková, I. C. Sampaio, S. Reich, *J. Phys. Chem. C* **2019**, *123*, 17498.
[26] C. Pfeiffer, C. Rehbock, D. Hühn, C. Carrillo-Carrion, D. J. de Aberasturi, V. Merk, S. Barcikowski, W. J. Parak, *J. R. Soc., Interface* **2014**, *11*, 20130931.
[27] T. Oncsik, G. Trefalt, M. Borkovec, I. Szilagyi, *Langmuir* **2015**, *31*, 3799.
[28] V. Merk, C. Rehbock, F. Becker, U. Hagemann, H. Nienhaus, S. Barcikowski, *Langmuir* **2014**, *30*, 4213.
[29] S. Kogikoski, A. Dutta, I. Bald, *ACS Nano* **2021**, *15*, 20562.
[30] A. Dutta, R. Schürmann, S. Kogikoski, N. S. Mueller, S. Reich, I. Bald, *ACS Catal.* **2021**, *11*, 8370.
[31] T. S. Marques, M. A. Śmiałek, R. Schürmann, I. Bald, M. Raposo, S. Eden, N. J. Mason, *Eur. Phys. J. D* **2020**, *74*, 222.
[32] T. S. Marques, R. Schürmann, K. Ebel, C. Heck, M. A. Śmiałek, S. Eden, N. Mason, I. Bald, *J. Chem. Phys.* **2020**, *152*, 124712.
[33] A. Dutta, R. Schürmann, I. Bald, *Eur. Phys. J. D* **2020**, *74*, 19.
[34] R. Schürmann, I. Bald, *Nanoscale* **2017**, *9*, 1951.
[35] J. Liu, Z.-Y. Cai, W.-X. Sun, J.-Z. Wang, X.-R. Shen, C. Zhan, R. Devasenathipathy, J.-Z. Zhou, D.-Y. Wu, B.-W. Mao, Z.-Q. Tian, *J. Am. Chem. Soc.* **2020**, *142*, 17489.
[36] P. C. Lee, D. Meisel, *J. Phys. Chem.* **1982**, *86*, 3391.
[37] I. Botiz, M.-A. Codescu, C. Farcau, C. Leordean, S. Astilean, C. Silva, N. Stingelin, *J. Mater. Chem. C* **2017**, *5*, 2513.
[38] C. Farcau, N. M. Sangeetha, H. Moreira, B. Viallet, J. Grisolia, D. Ciuculescu-Pradines, L. Ressier, *ACS Nano* **2011**, *5*, 7137.

[39] A. V. Delgado, F. González-Caballero, R. J. Hunter, L. K. Koopal, J. Lyklema, *Pure Appl. Chem.* **2005**, *77*, 1753.
[40] C. T. Gerold, C. S. Henry, *Langmuir* **2018**, *34*, 1550.
[41] B. Bera, N. Kumar, M. H. G. Duits, M. A. Cohen Stuart, F. Mugele, *Langmuir* **2018**, *34*, 13574.
[42] D. F. Parsons, M. Boström, P. L. Nostro, B. W. Ninham, *Phys. Chem. Chem. Phys.* **2011**, *13*, 12352.
[43] D. F. Parsons, M. Boström, T. J. Maceina, A. Salis, B. W. Ninham, *Langmuir* **2010**, *26*, 3323.
[44] B. W. Ninham, T. T. Duignan, D. F. Parsons, *Curr. Opin. Colloid Interface Sci.* **2011**, *16*, 612.
[45] K. D. Collins, *Biophys. Chem.* **2006**, *119*, 271.
[46] R. Kopelman, *Science* **1988**, *241*, 1620.
[47] N. G. Tognalli, E. Cortés, A. D. Hernández-Nieves, P. Carro, G. Usaj, C. A. Balseiro, M. E. Vela, R. C. Salvarezza, A. Fainstein, *ACS Nano* **2011**, *5*, 5433.
[48] A. Stefancu, O. M. Biro, O. Todor-Boer, I. Botiz, E. Cortés, N. Leopold, *ACS Photonics* **2022**, *9*, 895.
[49] A. Stefancu, S. Lee, L. Zhu, M. Liu, R. C. Lucacel, E. Cortés, N. Leopold, *Nano Lett.* **2021**, *21*, 6592.
[50] E. Cortés, W. Xie, J. Cambiasso, A. S. Jermyn, R. Sundararaman, P. Narang, S. Schlücker, S. A. Maier, *Nat. Commun.* **2017**, *8*, 14880.
[51] W. Nam, Y. Zhao, J. Song, S. Ali Safiabadi Tali, S. Kang, W. Zhu, H. J. Lezec, A. Agrawal, P. J. Vikesland, W. Zhou, *J. Phys. Chem. Lett.* **2020**, *11*, 9543.
[52] D. Steinigeweg, S. Schlücker, *Chem. Commun.* **2012**, *48*, 8682.